Journal of Earthquake Engineering
Publication details, including instructions for authors and subscription information:
http://www.tandfonline.com/loi/ueqe20

Capacity Design of Coupled RC Walls

Mr. Matthew James Fox[a], Dr. Timothy John Sullivan[b] & Dr. Katrin Beyer[c]

[a] ROSE Programme, UME School, IUSS Pavia, Italy

[b] University of Pavia, Department of Structural Mechanics, Pavia, Italy and EUCENTRE, Pavia, Italy

[c] École Polytechnique Fédérale de Lausanne, School of Architecture, Civil and Environmental Engineering, Lausanne, Switzerland

Accepted author version posted online: 19 Mar 2014.Published online: 19 Mar 2014.

To cite this article: Mr. Matthew James Fox, Dr. Timothy John Sullivan & Dr. Katrin Beyer (2014): Capacity Design of Coupled RC Walls, Journal of Earthquake Engineering, DOI: 10.1080/13632469.2014.904255

To link to this article: http://dx.doi.org/10.1080/13632469.2014.904255

Capacity Design of Coupled RC Walls

Author 1/Corresponding author: Mr. Matthew James Fox (matthew.fox@umeschool.it, +39 388 8238943), ROSE Programme, UME School, IUSS Pavia, Italy

Author 2: Dr. Timothy John Sullivan, University of Pavia, Department of Structural Mechanics, Pavia, Italy and EUCENTRE, Pavia, Italy

Author 3: Dr. Katrin Beyer, École Polytechnique Fédérale de Lausanne, School of Architecture, Civil and Environmental Engineering, Lausanne, Switzerland

Acknowledgements: The authors would like to thank Professor Nigel Priestley for his input at various stages of this research. The first author would also like to acknowledge the funding provided by the MEEES programme (www.meees.org).

Capacity design aims to ensure controlled ductile response of structures when subjected to earthquakes. This research investigates the performance of existing capacity design equations for reinforced concrete coupled walls and then proposes a new simplified capacity design method based on state-of-the-art-knowledge. The new method is verified through a case study in which a set of 15 coupled walls are subject to non-linear time-history analyses. The work includes examination of the maximum shear force in individual walls in relation to the total maximum shear force in the coupled wall system, and subsequently provides recommendations for design.

Keywords Reinforced concrete (RC), coupled walls, higher mode effects, capacity design.

1. Introduction

In multi-storey buildings, it is common to use reinforced concrete walls to resist part, or all, of the lateral forces generated by seismic or wind actions. Where two or more walls are connected by deep beams up their height they are termed a coupled wall. It is common that coupled walls

result from the necessity to have regular size penetrations in a wall at every floor level, as is shown in Figure 1. This results in two walls with regular size coupling beams at each floor level and it is this configuration that is the subject of this research.

The seismic response of coupled walls is fundamentally different to that of cantilever walls, in that two different mechanisms resist the overturning moment. Part is resisted by the walls in flexure and the remainder is resisted by an axial force couple in the walls, generated by the shear in the coupling beams. The proportioning of overturning moment resistance is defined by the coupling ratio, β, as expressed in Equation 1.

$$\beta = \left(\sum_{i=1}^{n} V_{CBi} \right) \left(L_{CB} + L_W \right) / M_{OTM} \qquad (1)$$

where V_{CBi} is the shear in a single coupling beam, L_{CB} is the coupling beam span, L_W is the length of the walls (two walls of equal length are assumed here) and M_{OTM} is the total overturning moment. A particularly critical aspect of the behaviour of coupled walls is the response of the coupling beams. For typical geometric configurations the rotational deformation demand on the coupling beams will be very large. This is problematic when conventionally reinforced coupling beams are used, as premature shear failure is likely to occur when the aspect ratio is low. As a solution to this problem, Paulay and colleagues at the University of Canterbury, New Zealand, developed the concept of diagonal reinforcing (Paulay, 1969; Paulay & Binney, 1974; Paulay & Santhakumar, 1976). Due to their superior performance, only diagonally reinforced coupling beams are considered in this research.

To investigate the capacity design requirements for coupled walls a review of three existing methods for capacity design is carried out, assessing the strengths and weaknesses of each method (Section 2). A new simplified capacity design method for coupled walls is then proposed (Section 3). The proposed method is then assessed through a case study application in which 15 different coupled walls are designed and then analysed using non-linear time-history analysis (Section 4). The paper closes with considerations on the shear and moment distribution between the coupled walls (Section 5).

2. Capacity design and a review of existing methods for coupled walls

2.1 Capacity design and intensity dependence

In the seismic design of new structures, the ground motion that a structure is likely to be subjected to is typically considered the largest source of uncertainty. Although predictions can be made based on previous events, there will never be certainty over the magnitude and characteristics of future earthquakes a structure may be subjected to. As explained originally in Park & Paulay (1975) and then in a more developed manner in Paulay & Priestley (1992), the philosophy of capacity design is intended to provide robustness to the structure and to some extent desensitise its response from the input ground motion.

The application of capacity design (as per Paulay & Priestley, 1992) to coupled wall structures with conventionally reinforced coupling beams requires the potential plastic hinge regions (at the

base of the walls and ends of the coupling beams) to be detailed for inelastic flexural action, and shear failure to be prevented by a suitable strength differential. The remaining portion of the walls and coupling beams are then also designed to have sufficient capacity to remain elastic and prevent shear failure and flexural yielding under actions corresponding to the development of the maximum feasible strength of the plastic hinges. When diagonally reinforced coupling beams are used, the coupling beam deforms inelastically along its full length and the whole coupling beam can be defined as a plastic region rather than having distinct plastic hinges at the ends. As the diagonally reinforced coupling beam behaves like a truss, no specific protection against shear failure is required.

To provide sufficient reserve strength to the necessary regions of the walls, the overstrength of the plastic hinges, compatibility forces and higher mode effects must be accounted for. In this paper, the combination of all three of these effects is considered to be what constitutes capacity design. This is in-line with the definitions provided by Park & Paulay (1975), Paulay & Priestley (1975) and Priestley *et al.* (2007). An alternative approach could be to consider that the capacity design accounts for only the effects of plastic hinge overstrength. This would require compatibility forces and higher mode effects to be considered in a later phase of design.

In this research, the focus is on higher mode effects. Typically higher mode effects are accounted for in design codes by a higher mode factor, which is independent of earthquake intensity. However, research (Eibl & Keintzel, 1988; Priestley & Amaris, 2002) has shown that forces due to higher mode effects are strongly intensity dependent and the plastic mechanism limits the forces associated to the first mode only. Therefore, the procedure of capacity design cannot be

deterministic but in fact must include probabilistic considerations to define a limiting intensity at which the desired ductile mechanism may no longer be maintained. As there is no clear definition of what earthquake intensity capacity design actions should relate to, all comparisons in this research are considered for both 100% and 200% of the design intensity. 200% of the design intensity has been used to represent what might correspond to the maximum credible event at a given site for a normal structure.

The significance of higher modes and their dependence on intensity can be seen in Figure 2, where the first mode wall shear forces and bending moments are plotted alongside values found from NTHA. Details of the 10-storey structure used in this example and the analyses will be presented in Section 4, but these results are shown here in order to emphasise the importance of higher modes for the response of coupled walls. Observe that shear and moment demands increase with intensity and that the total base shear forces are more than twice the 1st mode base shear force. There are various proposals in the literature to account for such higher mode effects and three of the most relevant for coupled walls will be reviewed in the next sub-sections. These are the NZS3101 (2006) method and methods by Priestley *et al.* (2007) and Pennucci *et al.* (2011).

2.2 NZS3101 (2006) method

The New Zealand Standard for the design of concrete structures, NZS3101 (2006), provides a method for the capacity design of reinforced concrete walls. As there is no specific method for

coupled walls, it is assumed that the method for cantilever walls can be applied. It should be noted that the same method for determining capacity design shear forces (but not bending moments) is provided in Paulay & Priestley (1992) and applied to coupled walls. In the NZS3101 method, capacity design shear forces, V^*_o, are determined using Equation 2.

$$V_o^* = \omega_v \phi^o V_E \qquad (2)$$

where ω_v is the dynamic shear magnification factor and is dependent on the number of storeys, ϕ^o is the overstrength factor related to flexural actions at the base of the wall and V_E is the shear force found from the analysis for seismic actions from an equivalent static analysis. The resulting capacity design shear force profile has the same shape as the first mode shear forces. From the points made in the previous section, it is therefore expected that the method will not give a good fit to the actual profile of shear forces once higher modes are accounted for. Capacity design bending moments are determined by constructing an envelope between zero moment at the top of the wall, a mid-height moment M^*_c given by Equation 3 and the nominal flexural strength at the base of the wall, $M_{n,B}$.

$$\frac{M_{n,B}}{2} < M_c^* = \frac{M_{E,C}}{0.85}\left[1+\frac{n-1}{4}\right] \le 2M_{E,C} \qquad (3)$$

where $M_{E,C}$ is the mid-height moment found from an equivalent static or modal response spectrum analysis and n is the number of storeys. An allowance must also be made for the effects of tension shift, which similarly applies to the other methods considered in this research. However, because tension shift is a simple phenomenon that can be accounted for through reinforced concrete mechanics, it will not be examined specifically here. Whilst the NZS3101

method is simple, it has a major drawback in that it does not account for earthquake intensity in any way. It is therefore unknown to the designer what allowance there is for earthquakes exceeding the design level.

2.3 Priestley et al. *(2007)* method

Priestley *et al.* (2007) do not provide a specific capacity design method for coupled walls, but state that the equations for cantilever walls can be conservatively applied to coupled walls. For shear forces, the first part of the capacity design method follows a similar form to that of the NZS3101 method, whereby the design base shear is multiplied by a dynamic amplification factor and an overstrength factor (as per Equation 4, which is identical in form to Equation 2, but with slightly different notation).

$$V^o_{Base} = \phi^o \omega_v V_{Base} \qquad (4)$$

where

$$\omega_v = 1 + \frac{\mu}{\phi^o} C_{2,T} \quad \text{and} \quad C_{2,T} = 0.067 + 0.4(T_i - 0.5) \le 1.15 \qquad (5,6)$$

In the next step though, the capacity design shear force at roof level is calculated (Equation 7) and then a linear envelope is constructed between the roof level and the base of the wall.

$$V^o_n = C_3 V^o_{Base} \quad \text{where} \quad C_3 = 0.9 - 0.3T_i \ge 0.3 \qquad (7,8)$$

It can be seen in Figure 2 (a) how an envelope of this shape would provide a superior fit to the NTHA results when compared to the NZS3101 method. The capacity design bending moments

are again calculated in a similar manner to the NZS3101 method where an envelope is constructed between the moments at the base of the wall, a specified moment at mid-height and zero moment at roof level. It should be noted though that the Priestley *et al.* method requires the designer to account for the flexural overstrength of the walls when determining the capacity design bending moments, which is not a requirement of the NZS3101 method.

Although the Priestley *et al.* method follows a similar format to the requirements of NZS3101 (2006) there are some major differences. Rather than characterizing higher mode effects by the number of storeys, Priestley *et al.* use the initial period of the wall, T_i , and the displacement ductility demand, μ. The incorporation of the ductility demand is particularly significant as it is used to account for increases in the response of higher modes as intensity increases. However, Sullivan (2010) argues that ductility demand might not be the best parameter by which to measure intensity since it does not account for the spectral shape and therefore may not adequately capture the relative intensity of higher modes.

There are some additional issues in applying the method to coupled walls. First, it is not known whether it should be the wall ductility demand or the system ductility demand used in the equations. Note that the system ductility demand is significantly larger than that of the walls alone, as it is driven up by the high ductility demand on the coupling beams. It was found in this research that better results were obtained using the wall ductility demand and so it is assumed this is the correct application. Second, the initial period of the structure may not be suitable for

characterising the behaviour of coupled walls, given the large reduction in stiffness that occurs in a coupled wall system once the coupling beams yield.

2.4 Pennucci et al. (2011) method

The Pennucci *et al.* (2011) method was developed for determining capacity design actions in tall coupled walls. It considers the shear forces and bending moments of each higher mode separately and then combines them with the fundamental mode using the square-root-sum-of-the-squares (SRSS) modal combination rule. The method is best explained by first considering the development of plasticity in coupled walls as shown in Figure 3. Different structural idealisations are used to account for higher mode characteristics and in particular period lengthening due to non-linear response, which, as explained by Sullivan *et al.* (2008), can have a significant effect on higher mode forces. When the structure is subjected to low intensity shaking, the higher modes are those of the elastic structure, as shown in Figure 3 (a). At an increased intensity it is assumed that all coupling beams develop large levels of ductility (a reasonable assumption for typical geometric configurations) and the higher modes then behave as two fixed base cantilevers, as in Figure 3 (b). As intensity increases further, the bases of the walls develop significant levels of ductility and the fixed base cantilevers transition towards becoming pinned base cantilevers, as shown in Figure 3 (c).

It is therefore possible to assume that each higher mode consists of a fixed base and a pinned base component. It is then assumed that the walls have constant flexural rigidity, *EI* and constant

distributed mass up their height. This facilitates the use of closed form equations for higher mode actions. The shear forces and bending moments due to higher modes can be found from Equations 9 and 10 respectively.

$$V_n = m\left[\rho c_{n,f} Sa_{n,f} + (1-\rho) c_{n-1} Sa_{n-1,p}\right] \quad (9)$$

$$M_n = mH\left[\rho d_{n,f} Sa_{n,f} + (1-\rho) d_{n-1} Sa_{n-1,p}\right] \quad (10)$$

where m is the total seismic mass resisted by the coupled walls, H is the height of the building and Sa is the spectral acceleration corresponding to a particular mode. The factors c and d are modal shear force and bending moment coefficients and ρ is a ductility dependent factor that equals one for an elastically responding structure and then decreases linearly to zero at a ductility of 3.5. Note that it is the displacement ductility demand on the walls that should be used, rather than the system ductility demand. The subscript n refers to the mode number and the subscripts f and p denote fixed or pinned base, respectively. The shear force envelope is constructed as a linear diagram between the base of the wall and mid-height and then the shear force is assumed constant up to roof level. The bending moment envelope is constructed between the moments calculated at the base of the walls, mid-height, 80% of the height and then roof level.

Even though the method is intended for tall buildings it was shown to apply to structures as low as 5 storeys with sufficient accuracy (Fox, 2013). By incorporating the spectral acceleration of each fixed or pinned based modal component into the equations, it directly accounts for earthquake intensity.

2.5 Summary of existing methods

Figures 4, 5 and 6 show an application of the three existing methods for determining capacity design actions that were considered in this research. The application is to the same 10 storey coupled wall with a 0.4 coupling ratio used in Figure 2. As discussed previously, comparisons are made at both 100% and 200% of the design intensity. The NZS3101 method gives the least favourable fit to the mean NTHA results, particularly for shear forces. The Priestley *et al.* method offers an improvement but it can be seen that there are still areas where the shear and moment envelopes do not fit particularly well. The Pennucci *et al.* method gives very good results for shear forces and reasonable results for bending moments. It must be noted however, that the Pennucci *et al.* method is more complex and requires significantly more design effort.

3. Proposed simplified method

3.1 Shear

The following method was developed as a simplified method for determining capacity design shear forces based on the work of Pennucci *et al.* (2011). The capacity design base shear and mid-height shear forces are calculated using Equations 11 and 12 respectively, where the coefficients C_2 and C_3 are obtained from Equations 14 and 15 as a function of the wall ductility demand and the factor C_1 calculated from Equation 13. The factor C_1 has some physical meaning in that it accounts for where the periods of the higher modes of vibration lie on the

design spectrum relative to the corner period T_C (between constant acceleration and constant velocity branches of the spectrum). For very low values of C_1 (very flexible structures) the method may be overly conservative, therefore, a practical lower bound on C_1 for the application of the proposed method is $0.17(T_C/T_D)^2$, where T_D is the corner period between the constant velocity and constant displacement branches of the design acceleration spectrum. The reasons for the limitation are discussed in Section 4.3. The factors C_2 and C_3 determine the level of shear coming from higher modes.

$$V_{base} = \sqrt{\left(\phi^o V_d\right)^2 + C_2\left(m.Sa_{PL}\right)^2} \tag{11}$$

$$V_{m-h} = \sqrt{\left(0.85\phi^o V_d\right)^2 + C_3\left(m.Sa_{PL}\right)^2} \tag{12}$$

$$C_1 = \frac{2T_C^2 EI}{mH_n^3} \tag{13}$$

$$C_2 = \min\begin{cases} 0.048 - 0.008\mu \\ (0.56 - 0.125\mu)(C_1 + 0.01) \end{cases} \tag{14}$$

$$C_3 = \min\begin{cases} 0.022 + 2\times10^{-4}\mu \\ (0.0019\mu - 2.8\times10^{-4})C_1 + 0.0026 \end{cases} \tag{15}$$

where Sa_{PL} is the pseudo spectral acceleration on the plateau (constant acceleration branch) of the design spectrum, EI is the flexural rigidity of a single wall (calculated from the secant stiffness to nominal yield), H_n is the total height of the structure and V_d is the design base shear. The wall ductility demand, μ, should not be taken as less than one nor should it be taken as

greater than 3.5. Once the capacity design base and mid-height shear forces have been determined, the shear envelope is constructed as per the Pennucci *et al.* method.

The proposed method was developed around three key simplifying assumptions. The first is that sufficiently accurate results can be obtained by considering only two higher modes. This is suitable for buildings of any height, noting that for buildings more than 15-20 storeys high the walls behave like a continuous beam (Pennucci *et al.*, 2011). The second assumption is that the acceleration spectrum is of the shape shown in Figure 7, where there is a constant acceleration branch up to a corner period, T_C, followed by a constant velocity branch up to a period, T_D. It is assumed that all periods corresponding to higher modes are less than T_D, so the spectrum beyond this point is irrelevant. This is consistent with the use of Newmark spectra typically provided in design codes.

The third key assumption is that the fixed and pinned base components of the higher modes can be assumed to lie in certain ranges of the acceleration spectrum depending on the period of the fixed and pinned base cantilevers (refer Figure 2 (b) and (c)). For 'short period' cantilevers ($C_1 \geq 0.12$) it is assumed that all higher mode components possess periods of vibration within the constant acceleration branch. For 'long period' cantilevers ($C_1 < 0.12$) it is assumed that the components of the first higher mode are on the constant velocity branch of the spectrum, while the components of the second higher mode are on the constant acceleration branch. This can be seen in Figure 7 where *f* and *p* indicate fixed or pinned base respectively and the numbers refer to the mode number. The first higher mode is made up of the second fixed (*2f*) and first pinned modes (*1p*) and the second higher mode is made up of the third fixed (*3f*) and second pinned (*2p*)

modes. These modal components can all be identified in Figures 3(b) and 3(c), which show the fixed and pinned based structures respectively. Note that in some cases when C_1 is close to 0.12, one of the first higher modes may lie slightly outside of the range of the spectrum it is assumed to be in (such as *1p* in Figure 7), but the resulting error is small and conservative. Referring back to Equations 14 and 15 it can now be noted that the top lines correspond to the 'short period' assumption and the bottom lines correspond to the 'long period' assumption. As both assumptions always give conservative results (relative to using the exact values of spectral acceleration) it is appropriate to take the minimum, as is done in Equations 14 and 15.

Further to the three key assumptions already used, an additional simplification is made and in doing so a number of factors required in the Pennucci *et al.* method are eliminated. It was observed that if the exact values for C_2 and C_3 were calculated using the Pennucci *et al.* [2011] approach, for a given value of C_1 their values varied almost linearly with ductility between values of μ=1 and μ=3.5. Above a ductility of 3.5 the values of C_2 and C_3 remain constant. From this observation the simplified equations for C_2 and C_3 can be obtained by determining the values of C_2 and C_3 at ductilities of one and 3.5 and then linearly interpolating between. For brevity only a single example of this procedure is examined here. Consider the case where it is assumed that the higher mode components *2f* and *1p* lie on the constant velocity branch of the spectrum. The equation for coefficient C_2 is obtained as follows:

First, the shear force at the base of the structure due to the first higher mode (n=2) is determined by substituting the appropriate values into Equation 9, which yields Equation 16. This is then squared to give Equation 17.

$$V_2 = m\left[1 \times 0.188 Sa_{2,f} + (1-1) \times 0.137 Sa_{1,p}\right] \quad (16)$$

$$V_2^2 = 0.188^2 m^2 Sa_{2,f}^2 \quad (17)$$

Now the spectral acceleration $Sa_{s,f}$ can be related to the plateau spectral acceleration using Equation 18.

$$Sa_{2,f} = Sa_{PL} \frac{T_C}{T_{2,f}} \quad (18)$$

where $T_{2,f}$ is the second mode period of vibration for a fixed base cantilever. $T_{2,f}$ is given by Equation 19,which can be derived from first principles (refer Chopra, 2006).

$$T_{2,f} = 0.285\sqrt{\frac{mH_n^3}{2EI}} \quad (19)$$

Now substituting Equations 18 and 19 into Equation 17 the following equation is obtained for the first higher mode base shear (squared):

$$V_2^2 = 0.435 C_1 m^2 Sa_{PL}^2 \quad (20)$$

The shear force due to the second higher mode (n=3) can then be found in the same manner. Note that in this case though, it is slightly more straight forward as the spectral acceleration is

assumed to be the plateau acceleration (refer Figure 7) and thus the C_1 term does not enter the equation.

$$V_3 = m\left[1 \times 0.065 \times Sa_{3,f} + (1-1) \times 0.04 \times Sa_{2,p}\right] \quad (21)$$

$$V_3^2 = 0.00423 m^2 Sa_{PL}{}^2 \quad (22)$$

and so the coefficient C_2 can be found by adding the two higher mode shears (squared) and dividing by $m^2 Sa_{PL}{}^2$, which gives:

$$C_2 = 0.435 C_1 + 0.00423 \quad (23)$$

The same procedure is repeated for a ductility of 3.5, which gives:

$$C_2 = 0.113 C_1 + 0.0016 \quad (24)$$

An expression for C_2 for any value of ductility between one and 3.5 can now be obtained by linear interpolation between Equations 23 and 24.

$$C_2 = (0.564 - 0.129\mu)C_1 + (0.00528\mu - 0.00105) \quad (25)$$

Finally, Equation 25 is simplified and rearranged to give Equation 26, which is the second line of Equation 14.

$$C_2 = (0.56 - 0.125\mu)(C_1 + 0.01) \quad (26)$$

3.2 Moment

It is feasible that simplified equations for capacity design bending moments could also be developed based around the Pennucci *et al.* method. However, this was not carried out as part of this research for two reasons. Firstly, in a preliminary study conducted by Fox~(2013), the fit of the Pennucci *et al.* method capacity design bending moment envelopes to the NTHA results was not as good as for shear demands. Secondly, the model used for NTHA verification of the methods allowed the walls to yield at any location up their height. This is not in-line with the typical application of capacity design whereby the regions of the walls above the potential plastic hinge region are required to remain elastic. Instead of ensuring the upper regions of the walls remain elastic, this research assumes that some low-level yielding is acceptable. Therefore, rather than considering capacity design bending moments, this research will investigate mid-height curvature ductility demands obtained when uniform longitudinal reinforcing is provided up the height of the walls. An upper limit will be tentatively set at μ_ϕ=3, which corresponds to the curvature ductility at which the concrete contribution to shear resistance in the modified UCSD model (Priestly *et al.*, 1996; Kowalsky & Priestley, 2000) begins to reduce.

It was found that when constant reinforcing is used up the height of the structure the curvature ductility in the upper half of the wall remained well below the aforementioned limit. It was therefore determined that an acceptable simplified approach is to use the same reinforcing up to 70% of the height of the structure. From here the flexural reinforcing can be gradually reduced up to the roof level. The moment capacity at roof level (in a single wall) should be greater than the moment given by Equation 27, which is equal to the shear force in a single coupling beam

acting on a lever arm from mid-span of the coupling beam to the centreline of the wall and then multiplied by an appropriate overstrength factor. The longitudinal wall reinforcing at roof level must also be sufficient to meet minimum reinforcing requirements, which may well govern.

$$M_{roof} = \phi^o \frac{\beta M_{OTM}}{2n} \quad (27)$$

The effects of reducing the reinforcing in this manner have not been assessed through NTHA. This should be carried out as part of a future study.

4. Case study application

To assess the sufficiency of the proposed simplified method for capacity design, a case study was carried out, in which a set of 15 coupled walls were designed and then analysed using NTHA. The results of the NTHA were then compared to the capacity design predictions.

4.1 Design

The set of 15 different coupled walls were designed using Direct Displacement-Based Design (DDBD). The designs were carried out in general accordance with the requirements of DBD12 (Sullivan *et al.*, 2012), which is based on the work of Priestley *et al.* (2007). In a number of steps, the design procedure used in this research deviated from DBD12 requirements. This related to how the height of contraflexure was determined and how the force-deformation response of the coupling beams was calculated. For further detail, the reader is referred to Fox (2013). Although DDBD has been used in this case, the proposed method is also applicable for

force-based design (FBD) because capacity design rules relate to plastic hinge strengths actually provided, irrespective of the method used to determine the strength levels. However, caution should be exercised as the proposed method incorporates the displacement ductility demand of the structure, which may not be determined with sufficient accuracy through FBD.

The set of 15 coupled walls consisted of three different coupling ratios (0.2, 0.4, 0.6) and five different building heights (5, 10, 15, 20, 30 storeys). The designs were all carried out for the simple idealised building in Figure 9 in which each coupled wall resists half the inertial forces in the direction being considered. Further details of each case study structure are provided in Appendix A. The design seismicity corresponded to the type 1 spectrum from Eurocode 8 – Part 1 (CEN, 2004) for ground type C and for a peak ground acceleration of 0.3g. The plateau of the spectrum was then reduced slightly so that it would better match the mean response of the selected accelerograms used for NTHA as described in the next section. As the corner period, T_D, used in EC8 is considered to be non-conservative (Priestley *et al.*, 2007), the constant velocity branch of the spectrum was extended out to a corner period of 8s, as seen in Figure 8, where the design spectrum is compared to response spectra for the set of accelerograms used for NTHA. Although the design spectrum used in this case was different from that of Eurocode 8 (CEN, 2004) the approach implicitly accounts for spectrum shape and therefore it is expected that the performance of the method would not be greatly affected. Consideration of different spectral shapes should form part of any future research.

4.2 Modelling and Analysis

The set of 15 coupled walls were analysed using non-linear time-history analysis in the program SeismoStruct V5.2.2 (Seismosoft, 2012). Distributed plasticity fibre-section elements were chosen to model the walls as they define explicitly the non-linearity at the material level. Such elements capture the moment-axial force interaction and axial elongation at the centroidal axis and these two points are considered particularly important for the analysis of coupled walls. A single displacement based element was used for each floor level with an additional element equal to the plastic hinge length used at the base of the wall (Yazgan & Dazio, 2010).

Tangent stiffness proportional damping was used with 3% of critical damping specified at the period corresponding to the second elastic mode of vibration (damping at mode *i* is then simply given by $\xi_i = \xi_2.T_2/T_i$). This decision was based on recommendations in literature (Priestley & Grant, 2005) and the findings of a sensitivity analysis. The sensitivity analysis considered three different damping models; tangent stiffness proportional, initial stiffness proportional and Rayleigh damping (using tangent stiffness). The results are shown in Figure 10. Once tangent stiffness proportional damping was selected, a further sensitivity analysis was conducted to assess the difference in response when 1%, 3% and 5% of critical damping were specified (results shown in Figure 11). The choice of 3% of critical damping was considered to be a compromise between the 5% typically assumed for reinforced concrete buildings and 0% as recommended by Petrini *et al.* (2008) for use with fibre-section models (although note that the recommendations made by Petrini *et al.* (2008) related to experimental testing of a bridge pier on a shake table and therefore excluded some sources of damping). Furthermore, as damping was specified at the

second mode the fraction of critical damping at the fundamental mode is in fact less than 3%. Ideally the elastic response of the structure should be compatible with average elastic spectrum for 5% damping, however, for fibre-element models the sections are initially uncracked and after cracking respond in a curvilinear fashion (as per a real RC section) rather than use a bi-linear idealisation. This makes the definitions of 'elastic response' and 'initial period' unclear. For these reasons, it is considered that the best means of specifying elastic damping for fibre-element analyses remains an open question requiring further research.

The distributed plasticity beam elements in SeismoStruct are rigid in shear and it was therefore necessary to implement additional transverse springs between the wall elements at each floor level. Although the shear stiffness of ductile walls is non-linear, previous studies on cantilever walls showed that linear springs yield reasonable estimates of the system's base shear (Beyer *et al.*, 2014). The stiffness of the springs was determined using Equation 28 from Beyer *et al.* (2011). The equation is semi-empirical and accounts for experimental evidence showing that the ratio of shear to flexural deformations in capacity designed walls remains relatively constant (Dazio *et al.*, 2009).

$$\frac{\Delta_s}{\Delta_f} = 1.5 \frac{\varepsilon_m}{\phi \tan \beta_{cr}} \frac{1}{H_n} \qquad (28)$$

where Δ_s and Δ_f are the shear and flexural deformations respectively, ϕ is the curvature, ε_m is mean axial strain, β_{cr} is the maximum crack inclination (assumed to be 45^o) and H_n is the shear span. A sensitivity analysis was carried out to assess the influence of variations in shear stiffness.

The calculated stiffness (100%) was compared with 50% and 200% of the calculated stiffness along with a model with no shear flexibility (rigid). The results are shown in Figure 12 where it can be seen that the variations in shear stiffness do not significantly affect the maximum shear force or bending moment profiles.

Once the computer models had been constructed, they were subjected to a set of 10 different natural ground motion records provided in Table 1. The ground motions were taken from Maley *et al.* (2013) and were scaled to match the displacement spectrum on average. An integration time-step of 0.01s was used.

4.3 Results for shear

The capacity design shear force envelopes for all 15 coupled walls were calculated for both 100% and 200% of the design intensity and compared to the results of the time-history analyses. All NTHA results presented from herein are the mean of the 10 ground motions. For the ductility dependent shear estimates at 200% of the design intensity, it was assumed that the wall ductility could be calculated taking the displacement of the equivalent single-degree-of-freedom system as twice the displacement at the design intensity. Selected results are presented in Figure 13 showing the shear forces up the height of the structure.

The first three walls (Figure 13 (a), (b) and (c)) show a very good comparison between the NTHA results and the capacity design shear envelope. For the fourth wall (Figure 13 (d)) the shear forces found from the NTHA are much less than the design prediction. The reason for this gross conservatism is due to the third assumption, relating to the location of higher modes on the acceleration spectrum, no longer being valid. As explained in Section 3.1, it is assumed in this simplified approach that the components of the second higher mode are located on the plateau of the acceleration spectrum. In reality, due to the low stiffness of the cantilevers (a result of a large number of storeys and low coupling ratio) the components of the second higher mode are in fact on the constant velocity branch of the spectrum. Thus the shear forces due to the second higher mode are over predicted and the capacity design envelope becomes very conservative. It is therefore recommended that for $C_1<0.17(T_C/T_D)^2$ the designer should use an alternative method such as that of Pennucci *et al.* (2011) or NTHA. For the set of structures analysed, this corresponded to only the one case, which was the 30 storey building with a coupling ratios of 0.6. This is identified in Figure 14, where the proposed simplified method and the NTHA results are compared for base shear and maximum upper half shear, for all 15 coupled walls at 200% of the design intensity. Results are expressed in terms of the ratio of predicted shear to NTHA shear and the term 'upper half' is used to define the constant shear region of the capacity design envelope from mid-height to roof level.

Figure 15 shows a comparison between capacity design shear forces determined using the simplified method and the Pennucci *et al.* method. This is a useful comparison as it identifies the

level of error generated by the assumptions necessary to develop the simplified method. It can be seen that generally the error is very small, typically within 10% and tends to be more on the conservative side. The one major exception is the 30 storey building with the 0.6 coupling ratio, for reasons discussed previously.

4.4 Curvature

As discussed previously, the simplified capacity design strategy for flexure was to control the curvature rather than ensure elastic response in the upper regions of the wall. Figure 16 shows an example of the maximum curvatures up the height of the walls for 100% and 200% of the design intensity. It can be seen that at the design intensity the upper regions of the wall do not yield but at 200% of the design intensity the yield curvature limit is exceeded. The yield curvature has been determined using simplified equations from Priestley *et al.* (2007). It was found that generally peak curvature concentrated at the base plastic hinge and around the mid-height of the walls as can be seen in Figure 16. It was therefore deemed appropriate to consider the curvature limit as applying to the upper half of the wall as this would include the mid-height peak. It should be noted that the majority of inelastic behaviour is concentrated in a single element equal to the plastic hinge length at the base of the wall and within this element the curvature remains relatively constant. Although this does not reflect the true behaviour of a reinforced concrete wall, it was a necessary simplification to the modelling strategy (refer Fox (2013) for further details).

For all 15 walls the maximum curvature ductility in the upper half of the walls was determined by dividing the curvature obtained from NTHA with the yield curvature estimated by the simplified equations from Priestley *et al.* (2007). The results are shown in Figure 17 for 100% and 200% of the design intensity.

The largest curvature ductility from all the walls is 2.5, which is below the tentative upper limit of 3.0. For a number of walls, the strategy of using the same reinforcing up the height of the wall appears to be too conservative. In particular for the taller walls, which generally have a lower displacement ductility demand. However, it can be seen that at 200% intensity nine of the 15 walls yield in their upper half. Therefore, if the design objective for these cases was for the upper regions to remain elastic (traditional capacity design objective), then it would be necessary to have more reinforcing in the upper regions of the wall than at the base. From the results presented, it appears that the proposed recommendations are generally appropriate except for tall buildings. Clearly the sufficiency of the method is also dependent on what intensity level is being considered for capacity design.

5. Actions in individual walls

Up to this point, only the total shear force in the coupled walls has been considered. For design, it is necessary to provide sufficient capacity to each wall individually and therefore the demand

must be known in each individual wall. In coupled walls, the total bending moment and shear force demands are not distributed evenly between the two individual walls, due to the different axial loads induced by the coupling beams. It would seem initially obvious that the most logical way to determine the maximum shear force in an individual wall would be to distribute the total shear in proportion to the moment capacity at the base of each wall. This is the approach adopted in Paulay & Priestley (1992) and can be expressed by Equation 29.

$$V_{Ind} = V_{Sum}\left(\frac{M_C}{M_C + M_T}\right) \qquad (29)$$

where V_{Ind} is the maximum shear in an individual wall, V_{Sum} is the maximum total shear force in the coupled wall system and M_C and M_T are the moment capacities of the individual walls, in compression and tension respectively, once all coupling beams have yielded. This method was applied to the set of coupled walls to determine the maximum base shear and maximum shear force in the upper half of the walls at 200% of the design intensity. The total shear force in the walls was found using the newly proposed method and then Equation 29 was used to predict the maximum shear force in an individual wall. This was then compared to the maximum shear force in an individual wall found directly from the NTHA results. However, to provide for a better comparison, the individual wall shears found from the NTHA were scaled by the ratio of total NTHA shear to total predicted shear. This ensured that any errors associated with the simplified approach in predicting the NTHA results were eliminated and instead the focus remained on the relationship between the totalshear in a coupled wall system and the maximum shear force in an individual wall. The results are expressed as the ratio of the predicted shear to the NTHA shear found directly and therefore values greater than unity are conservative.

Figure 18 shows that generally the use of Equation 29 is rather conservative for the upper half shear. It was hypothesised that more accurate results could be obtained by considering the shear force contributions from each mode separately. Considering first the fundamental mode, it is obvious that the behaviour is strongly influenced by the strength (or equivalently flexural rigidity, *EI*) at the base of the walls. It is therefore rational to proportion the shear forces due to the fundamental mode using Equation 29. Now considering the higher modes, it can be shown in a qualitative manner (with reference to Figures 19 and 20) that this method is no longer rational. The bending moment diagrams for the first two higher modes are shown in Figure 19 for both the fixed and pinned base cases. It can be seen that there are a number of peaks in the bending moment diagrams up the height and therefore the response is more related to the stiffness distribution over the full height of the wall. In the upper regions of the walls, the difference in *EI* between the two walls is not as significant (as shown in Figure 20) and therefore the shear forces due to higher modes should be more evenly distributed between the walls than the fundamental mode shears.

On this basis, it was proposed that higher mode shear forces (considering here only two higher modes) could be split more evenly between the two walls. The best results were obtained distributing 55% and 50% of the total higher mode shear forces to an individual wall for the base shear and mid-height shear respectively. This is reflected in Equations 30 and 31, which give the base and mid-height shears for an individual wall using the newly proposed method.

$$V_{base,ind} = \sqrt{\left(\frac{M_C}{M_C + M_T}\phi^o V_d\right)^2 + C_2\left(0.55m.Sa_{PL}\right)^2} \qquad (30)$$

$$V_{m-h,ind} = \sqrt{\left(\frac{0.85M_C}{M_C + M_T}\phi^o V_d\right)^2 + C_3\left(0.5m.Sa_{PL}\right)^2} \qquad (31)$$

Equations 30 and 31 were applied to the set of 15 coupled walls at 200%. The results are shown in Figure 21 for the base shear and upper half shear. They give a very good prediction of the shear in an individual wall.

Having determined the shear demand in an individual wall, some discussion of shear capacity is warranted. The shear capacity of a reinforced concrete wall is dependent on the axial force and this is reflected in a number of models such as the modified UCSD model (Priestley *et al.*, 1996; Kowalsky & Priestley, 2000). This is problematic as the axial force in an individual wall is not strictly known at the time when the maximum shear force occurs. Furthermore, the critical condition may not be when the maximum shear force occurs but instead at an instant in time when the shear capacity is reduced due to an unfavourable axial load state. In light of this, it is recommended that the most conservative axial load condition be assumed when checking the shear capacity. The same issue arises when considering bending moments as the moment capacity is dependent on axial load. However, because the proposed method considers reinforcing content directly, rather than moment capacity, this problem is avoided.

6. Conclusions

This research has assessed a number of existing capacity design methods for RC coupled walls by comparing shear forces and bending moments found from the capacity design equations against the results of non-linear time-history analyses. Three existing methods were considered; those of NZS3101, Priestley *et al.* (2007) and Pennucci *et al.* (2011). From the existing methods Pennucci *et al.* (2011) gave the best results and was subsequently used to develop a simplified method for determining the capacity design shear forces in coupled walls. The proposed method was then verified through a case study application. An equivalent method for bending moments was not developed but instead it was shown that using constant reinforcing up the height of the structure could keep curvature ductility at the mid-height of the wall within a proposed limit of μ_ϕ=3.0. Having determined the maximum shear forces in the coupled wall system, it was shown that the maximum shear force in an individual wall could be found by distributing the fundamental mode shear forces in proportion to the moment capacity at the bases of the walls and the higher modes shear force split evenly between the walls.

Throughout this work it became evident that further research is necessary in a number of areas:

- The effects of interaction between the floor slab and coupling beams was not considered in this research as it was not expected to affect the outcomes, at least in a conceptual sense. However, for a practical design it is necessary to incorporate these effects and further research is required to clearly define a solution to this issue.

- Given the level of current knowledge on the relationship between capacity design actions and earthquake intensity it seems that further research is required to determine what earthquake intensity capacity design actions should relate to.

- If some limited yielding is to be permitted in the mid-height regions of reinforced concrete walls then it is necessary to define appropriate limits. Future research should seek to define curvature ductility limits for the mid-height regions of walls and address potential stability issues.

- This research has been limited to the consideration of simple structures. Further research is required to determine how the proposed approach could be applied to more complex structures, for example, structures with multiple coupled walls or dual systems.

References

Beyer, K., Dazio, A., Priestley, M.J.N. (2011) "Shear Deformations of Slender Reinforced Concrete Walls under Seismic Loading," *ACI Structural Journal*, Vol. 108, No. 2, pp. 167-177.

Beyer, K., Simonini, S., Constantin, R., Rutenberg, A. (2014) "Seismic shear distribution among interconnected cantilever walls of different lengths," *Earthquake Engineering and Structural Dynamics, accepted.*

Chopra, A.K. (2006) *Dynamics of Structures*, Prentice Hall, 3rd edition, New Jersey.

Comité Européen de Normalisation, "Eurocode 8, Design of Structures for Earthquake Resistance – Part 1: General Rules, Seismic Actions and Rules for Buildings," EN 1998-1, CEN, Brussels, Belgium, 2004.

Dazio, A., Beyer, K., Bachmann, H. (2009) "Quasi-Static cyclic tests and plastic hinge analysis of RC walls," *Engineering Structures*, Vol. 31, No. 7, pp. 1556-1571.

Eible, J., Keintzel, F. (1988) "Seismic Shear Forces in RC Cantilever Shear Walls," *Proceedings, 9th World Conference on Earthquake Engineering,* Tokyo/Kyoto, Japan.

Fox, M.J. (2013) "Seismic Design of Coupled Walls," *Master Thesis*, ROSE Programme, UME School, IUSS Pavia, Ialy.

Maley, T., Sullivan, T.J., Lago, A., Roldan, R. (2013) (in press) *Characterising the Seismic Behaviour of Steel Moment Resisting Frame Structures*, IUSS Press, Pavia, Italy.

NZS3101 (2006) " Concrete Structures Standard – Part 1 (Code) and Part 2 (Commentary)", Standards New Zealand.

Kowalsky, M.J., Priestley, M.J.N., "An improved analytical model for shear strength of circular RC columns in seismic regions," *ACI Journal*, Vol. 97(3), 2000, pp. 388-396.

Park, R., Paulay, T. (1975) *Reinforced Concrete Structures*, Wiley, New York.

Paulay, T. (1969) "The Coupling of Shear Walls," *Doctoral Thesis,* University of Canterbury, New Zealand.

Paulay, T., Binney, J.R. (1974) "Diagonally Reinforced Coupling Beams of Shear Walls," *Publication SP-42,* American Concrete Institute, pp. 579-598.

Paulay, T., (2002) "The displacement capacity of reinforced concrete coupled walls," *Engineering Structures*, 24, pp. 1165-1175.

Paulay, T., Priestley, M.J.N. (1992) *Seismic Design of Reinforced Concrete and Masonry Buildings*, Wiley, New York.

Pennucci, D., Sullivan, T.J., Calvi, G.M. (2011) *Performance-Based Seismic Design of Tall RC Wall Buildings*, IUSS Press, Pavia, Italy.

Petrini, L., Maggi, C., Priestley, M.J.N., Calvi, G.M. (2008) "Experimental Verification of Viscous Damping Modeling for Inelastic Time History Analyzes," *Journal of Earthquake Engineering*, Vol.12, Supplement 1.

Priestly, M.J.N., Seible, F., Calvi, G.M. (1996) *Seismic Design and Retrofit of Bridges*, Wiley, New York.

Priestley, M.J.N., Amaris, A.D. (2002) *Dynamic Amplification of Seismic Moments and Shear Forces in Cantilever Walls,* IUSS press, Pavia, Italy.

Priestley, M.J.N., Grant, D.N. (2005) "Viscous Damping in Seismic Design and Analysis," *Journal of Earthquake Engineering,* Vol. 9(SP2), 2005.

Priestley, M.J.N, Calvi, G.M., Kowalsky, M.J. (2007) *Displacement-Based Seismic Design of Structures*, IUSS Press, Pavia Italy.

Seismosoft (2012) *SeismoStruct: A Computer Program for Static and Dynamic Nonlinear Analysis of Framed Structures*, Version 5.2.2, http://www.seismosoft.com.Sullivan, T.J. (2010) "Capacity design considerations for RC frame-wall structures", *Earthquakes and Structures,* Vol. 1, No. 4, pp. 391-410.

Sullivan, T.J., Calvi, G.M., Priestley, M.J.N. (Editors) (2012) *A Model Code for the Displacement-Based Seismic Design of Structures DBD12*, IUSS Press, Pavia, Italy.

Sullivan, T.J., Priestley, M.J.N., Calvi, G.M., (2008) "Estimating the Higher Mode Response of Ductile Structures," *Journal of Earthquake Engineering*, Vol. 12, No. 3, pp. 456-472.

Vecchio, F.J., Collins, M.P. (1986) "The Modified Compression-Field Theory for Reinforced Concrete Elements Subjected to Shear," *ACI Journal,* Proceedings V. 83, No. 2, Mar.-Apr., pp. 219-231.

Yazgan, U., Dazio, A. (2010) "Critical Aspects of Finite Element Modeling of RC Structures for Seismic Performance Assessment," *Proceedings of the 9th U.S. National and 10th Canadian Conference on Earthquake Engineering*, Paper No. 404, Toronto, Canada.

Appendix A – Details of case study structures

Additional symbols used in Appendix A:

t_w: Wall thickness

h_{CB}: Coupling beam depth

N_{grav}: Axial load on a single wall due to gravity loads

T_1: Fundamental period of building considering cracked section stiffness

T_e: Effective period of structure determined from DDBD

K_e: Effective stiffness of structure determined from DDBD

V_b: Design base shear of coupled wall from DDBD

M_{wall}: Design bending moment at base of an individual wall from DDBD

N_{eq}: Axial load on a single wall due to earthquake loading

$A_{s,CB}$: Area of coupling beam diagonal reinforcing

ρ_w: Wall longitudinal reinforcing ratio

FIGURE 1 Common configuration of coupled walls (reproduced with permission from Paulay & Priestley, 1992).

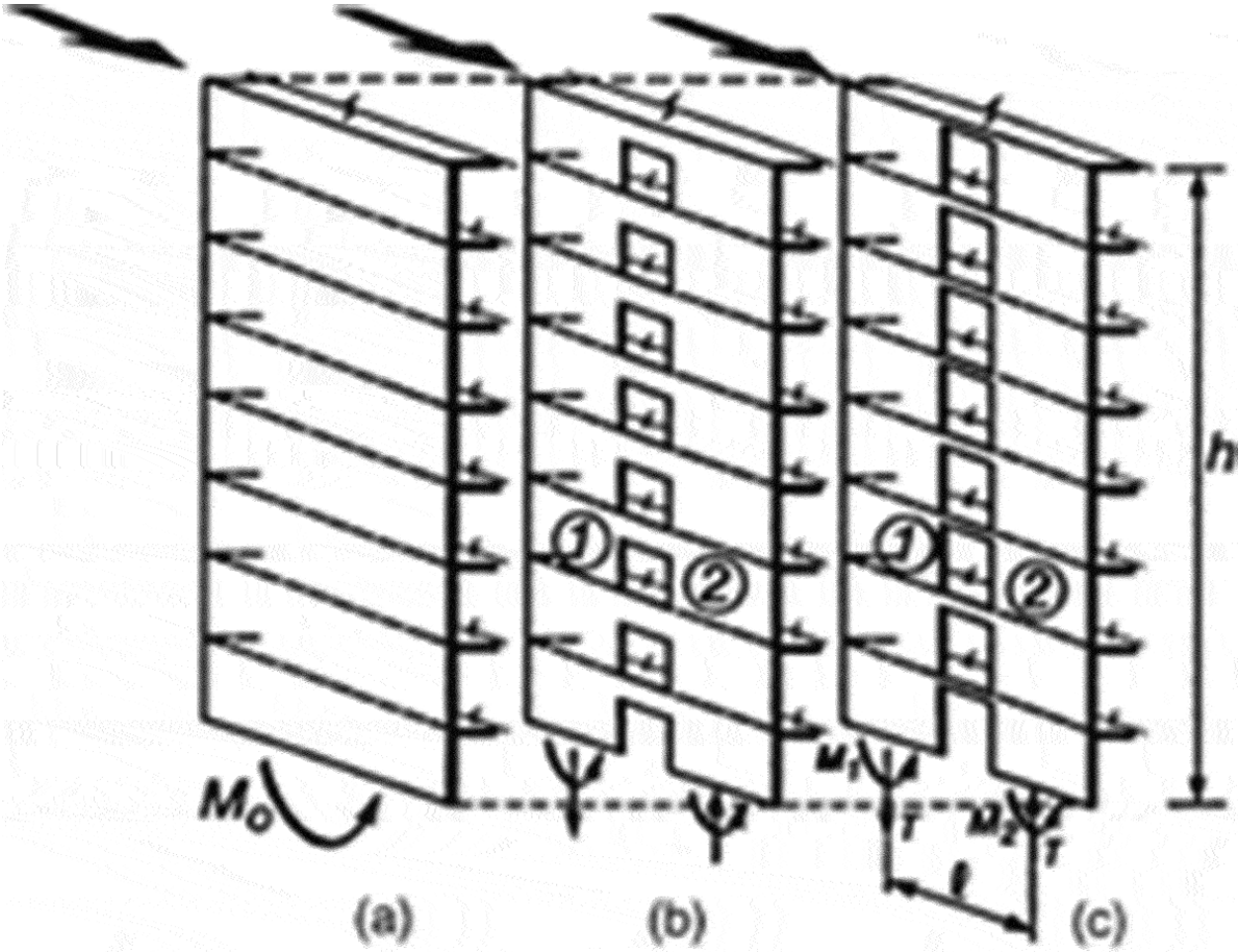

FIGURE 2 Comparison of first mode response and NTHA results for (a) shear force (b) bending moment in a 10 storey coupled wall with a 0.4 coupling ratio.

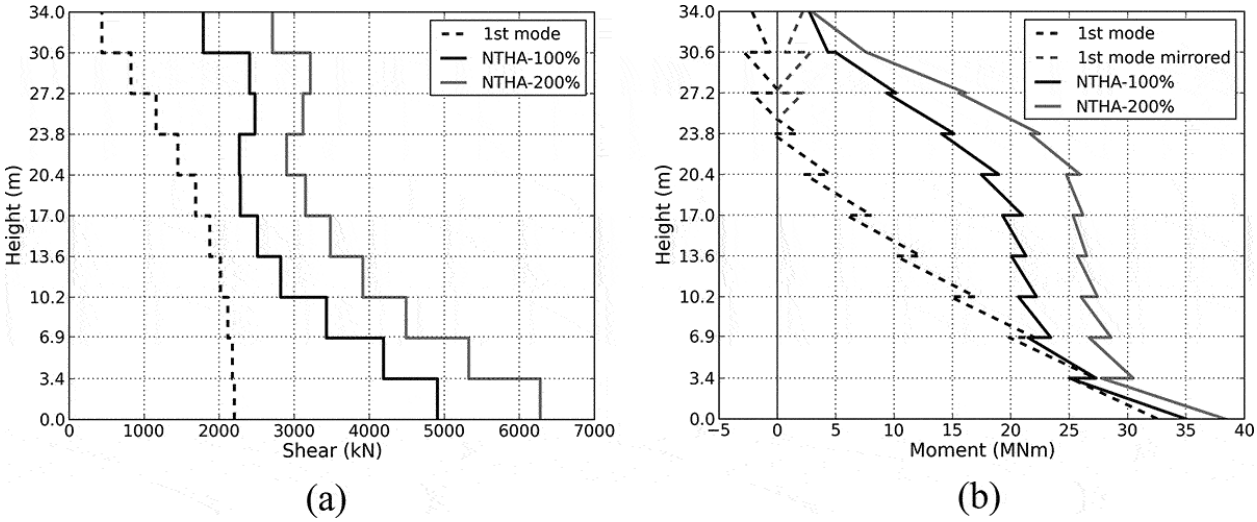

FIGURE 3 Development of ductility in a coupled wall structure from (a) low intensity, to (b) medium intensity, to (c) high intensity (adapted from Pennucci et al., 2011) and corresponding mode shapes (d), (e) and (f). Note that the sway mode for the high intensity case is not identified as it is unstable.

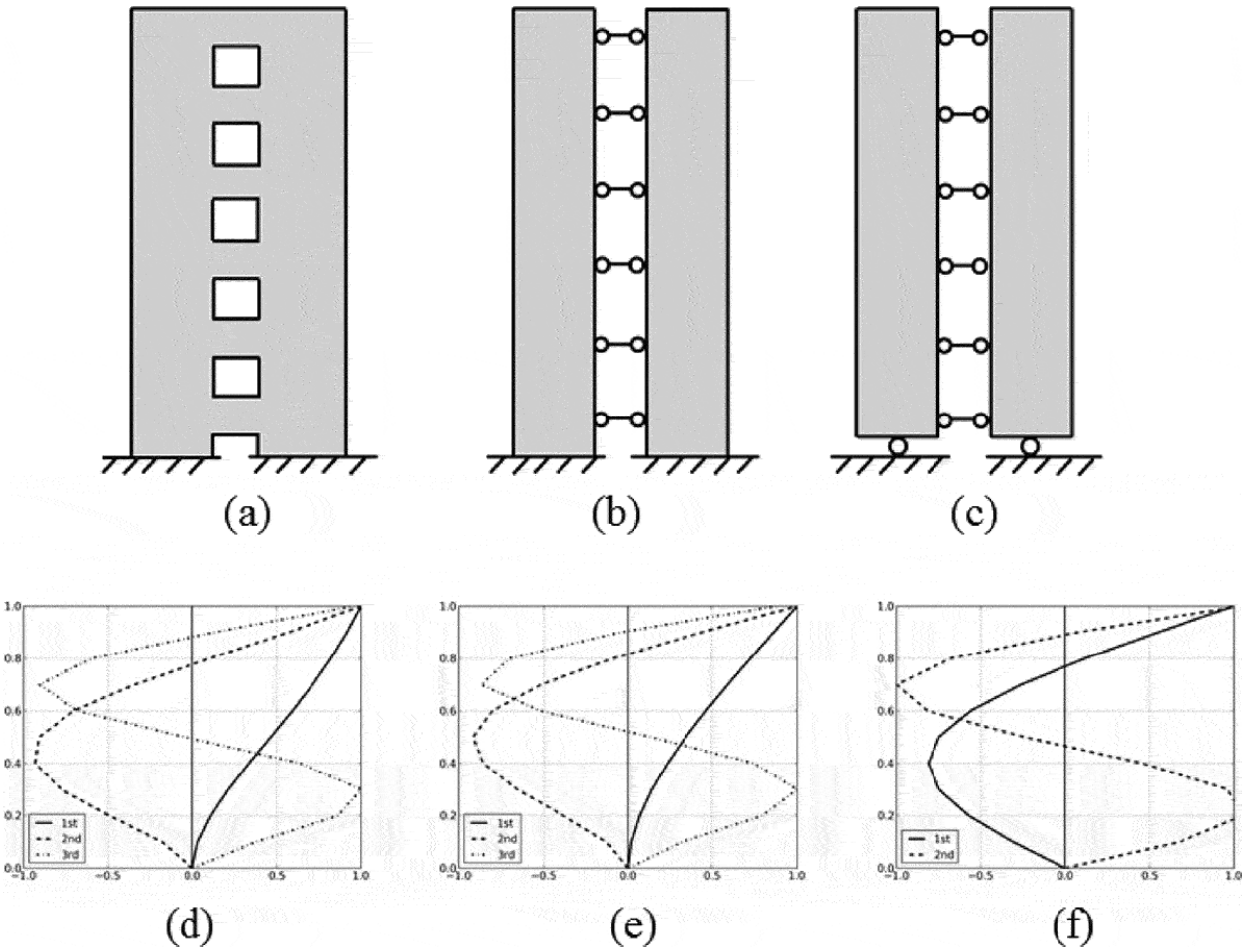

FIGURE 4 NZS3101 capacity design actions (a) shear (b) moment.

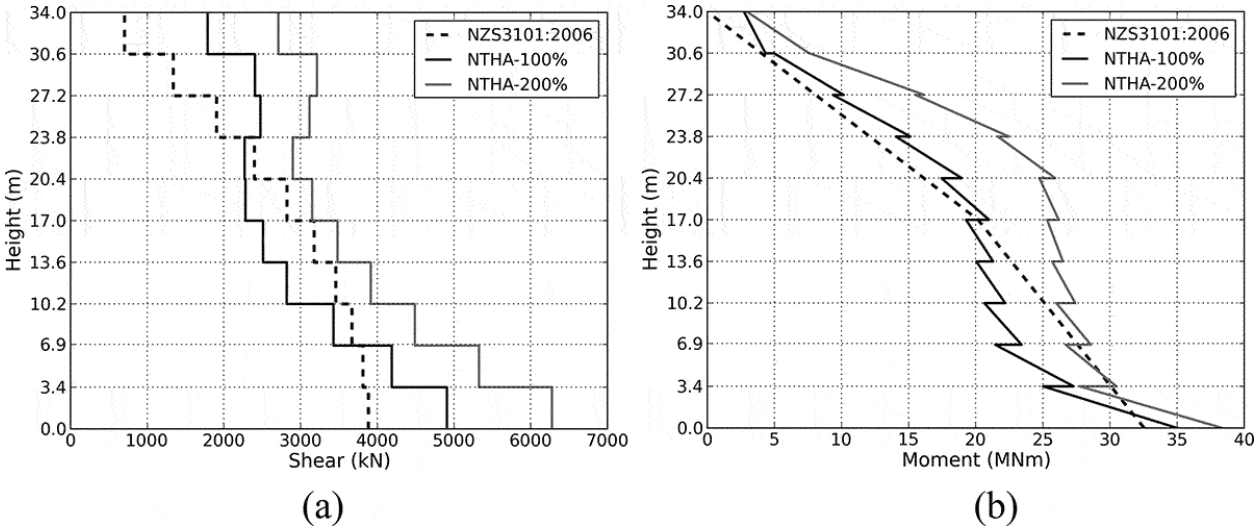

FIGURE 5 Priestley et al. (2007) capacity design actions (a) shear (b) moment.

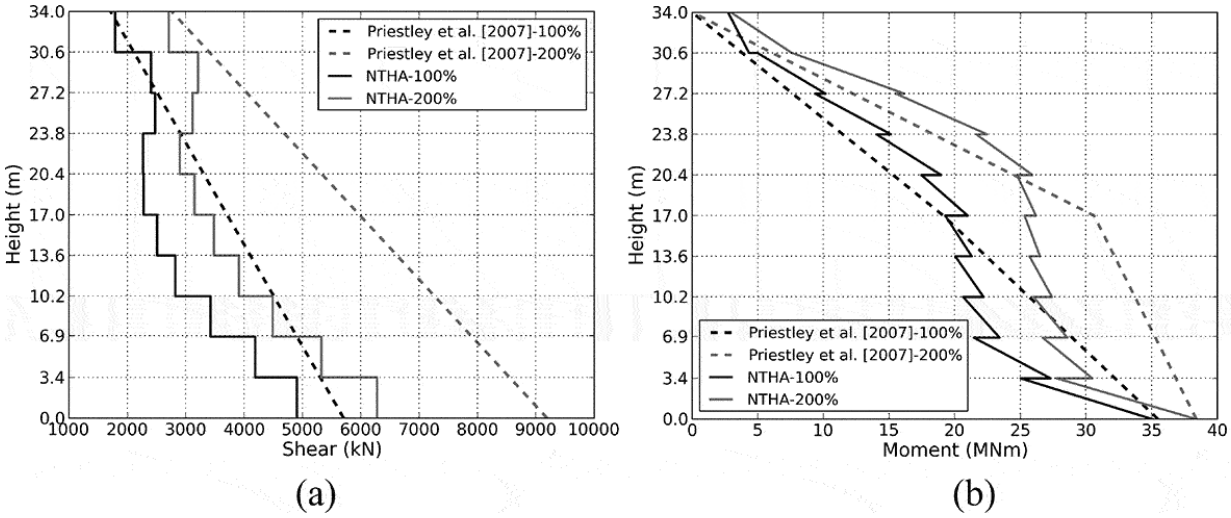

FIGURE 6 Pennucci et al. (2011) capacity design actions (a) shear (b) moment.

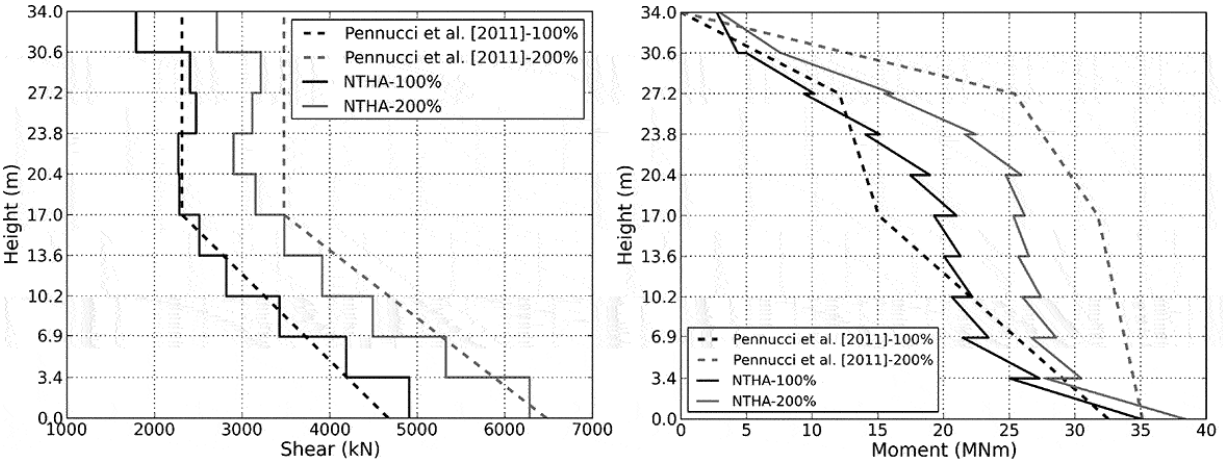

FIGURE 7 Example of assumed location of higher mode components on the acceleration spectrum.

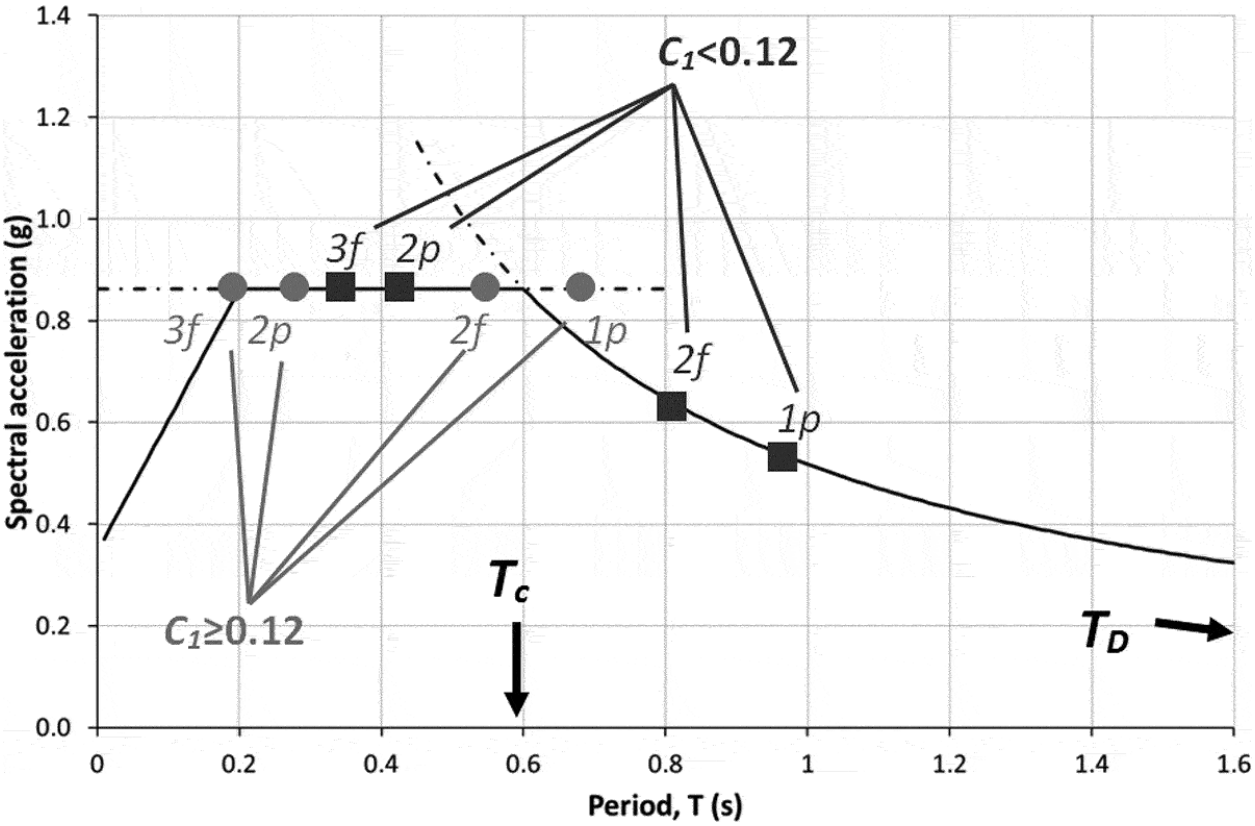

FIGURE 8 Displacement and acceleration design and response spectra.

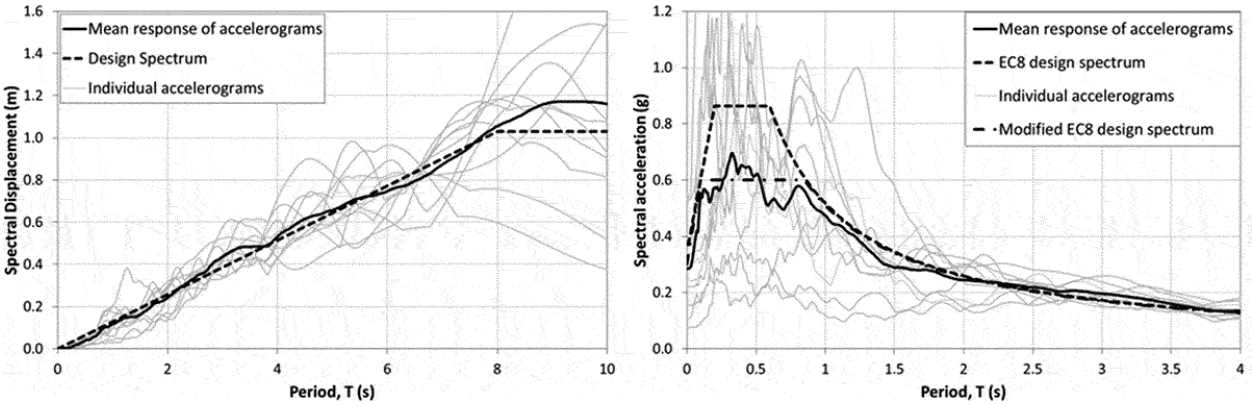

FIGURE 9 Case study building.

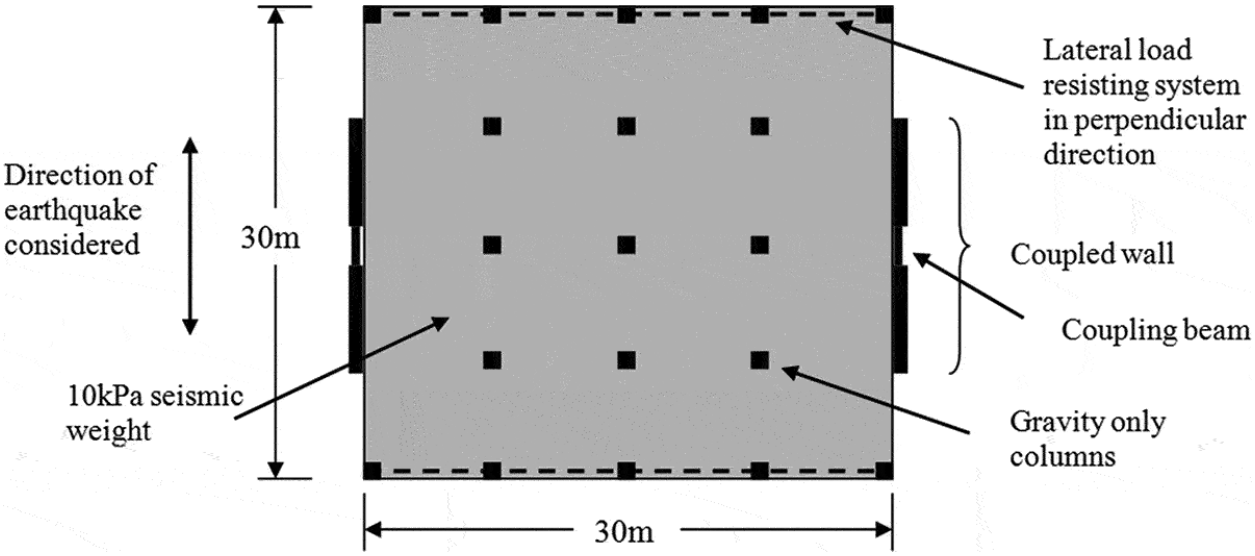

FIGURE 10 Results of sensitivity analysis for different elastic damping models (a) shear (b) moment.

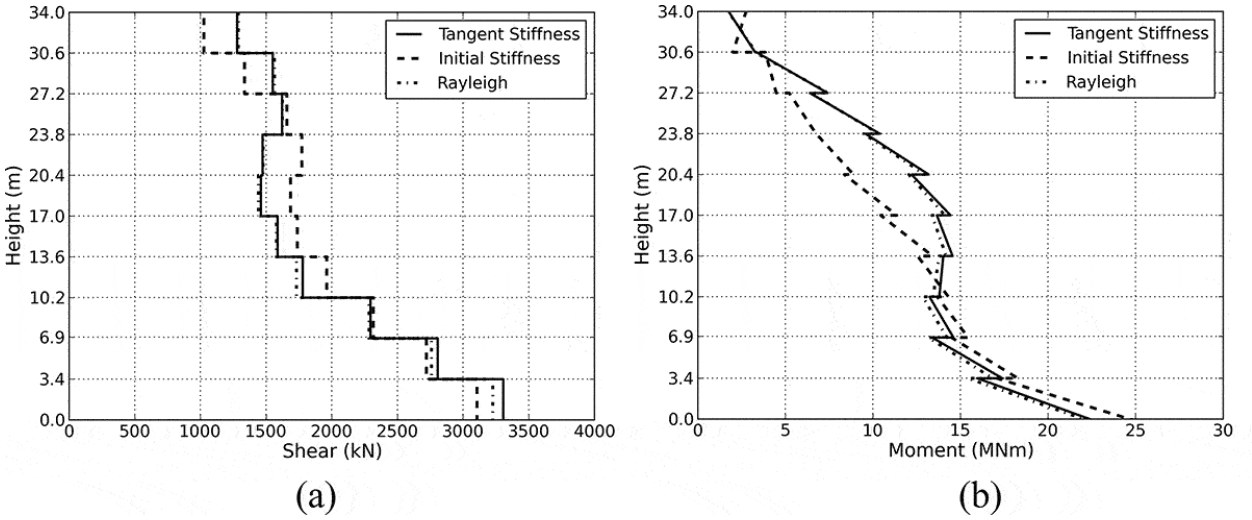

FIGURE 11 Results of sensitivity analysis for different damping ratios using tangent stiffness proportional damping (a) shear (b) moment.

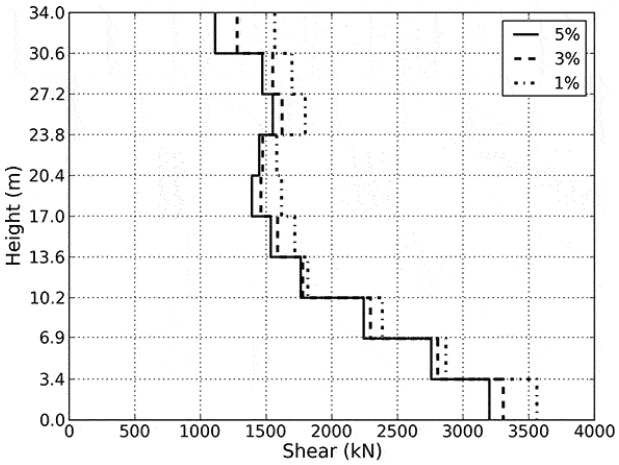

(a)

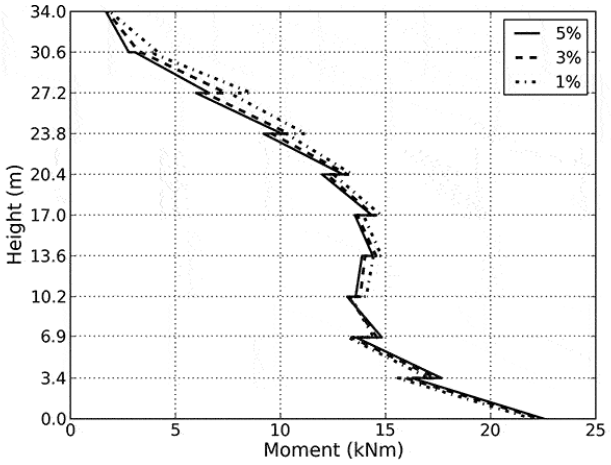

(b)

FIGURE 12 Results of sensitivity analysis for different values of shear stiffness (a) shear (b) moment.

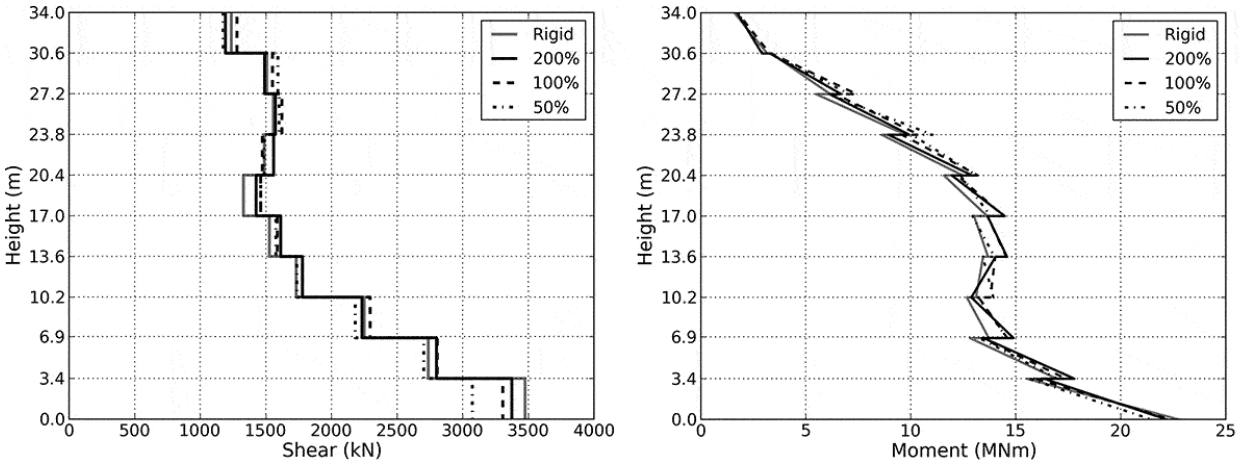

FIGURE 13 Comparison of NTHA shear forces and simplified capacity design prediction for representative sample.

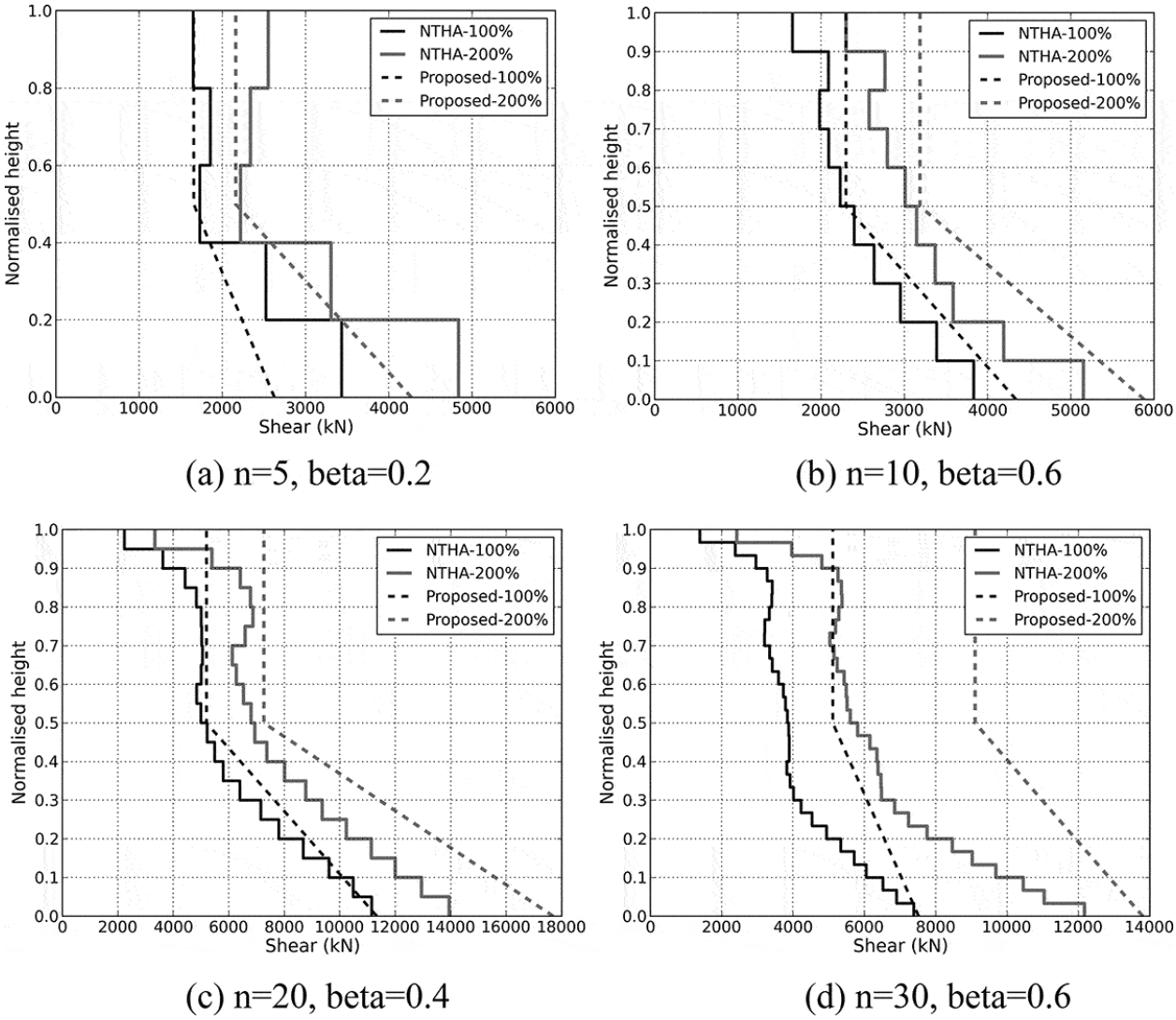

FIGURE 14 Comparison of NTHA shear forces and simplified capacity prediction for (a) base shear (b) maximum upper half shear at 200% of the design intensity.

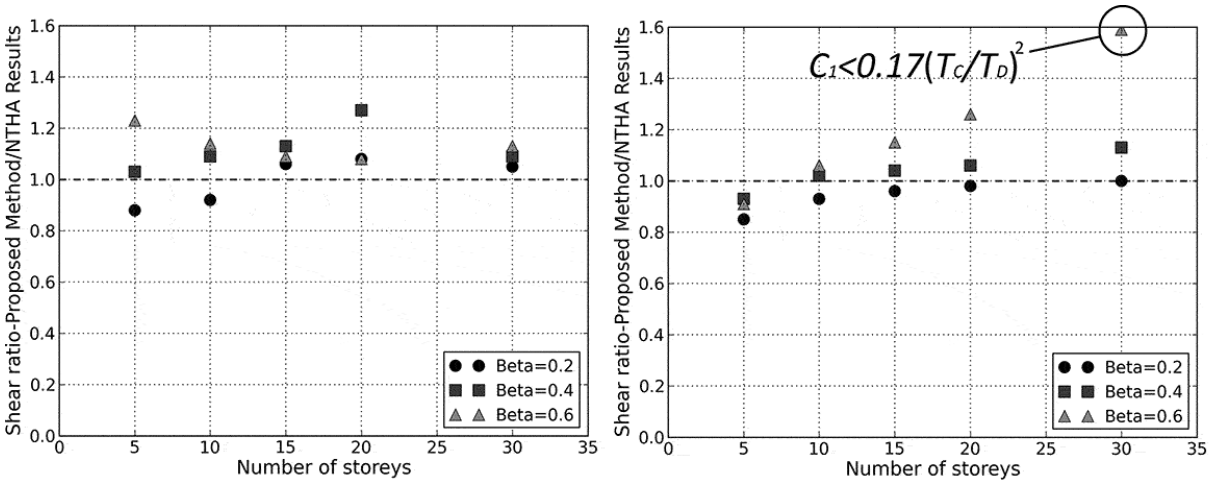

FIGURE 15 Comparison of Pennucci et al. shear forces and simplified capacity design prediction for (a) base shear (b) maximum upper half shear at 200% of the design intensity.

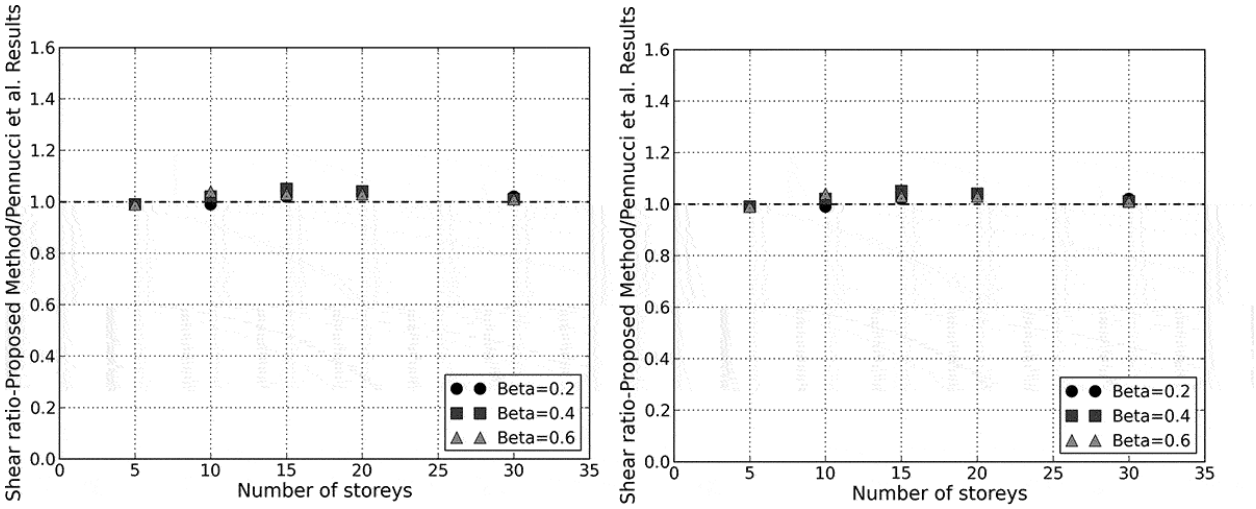

FIGURE 16 Curvature profiles from NTHA results for the 10 storey wall with 0.4 coupling ratio at 100% and 200% of the design intensity (maximum base curvature of 0.030 m not shown).

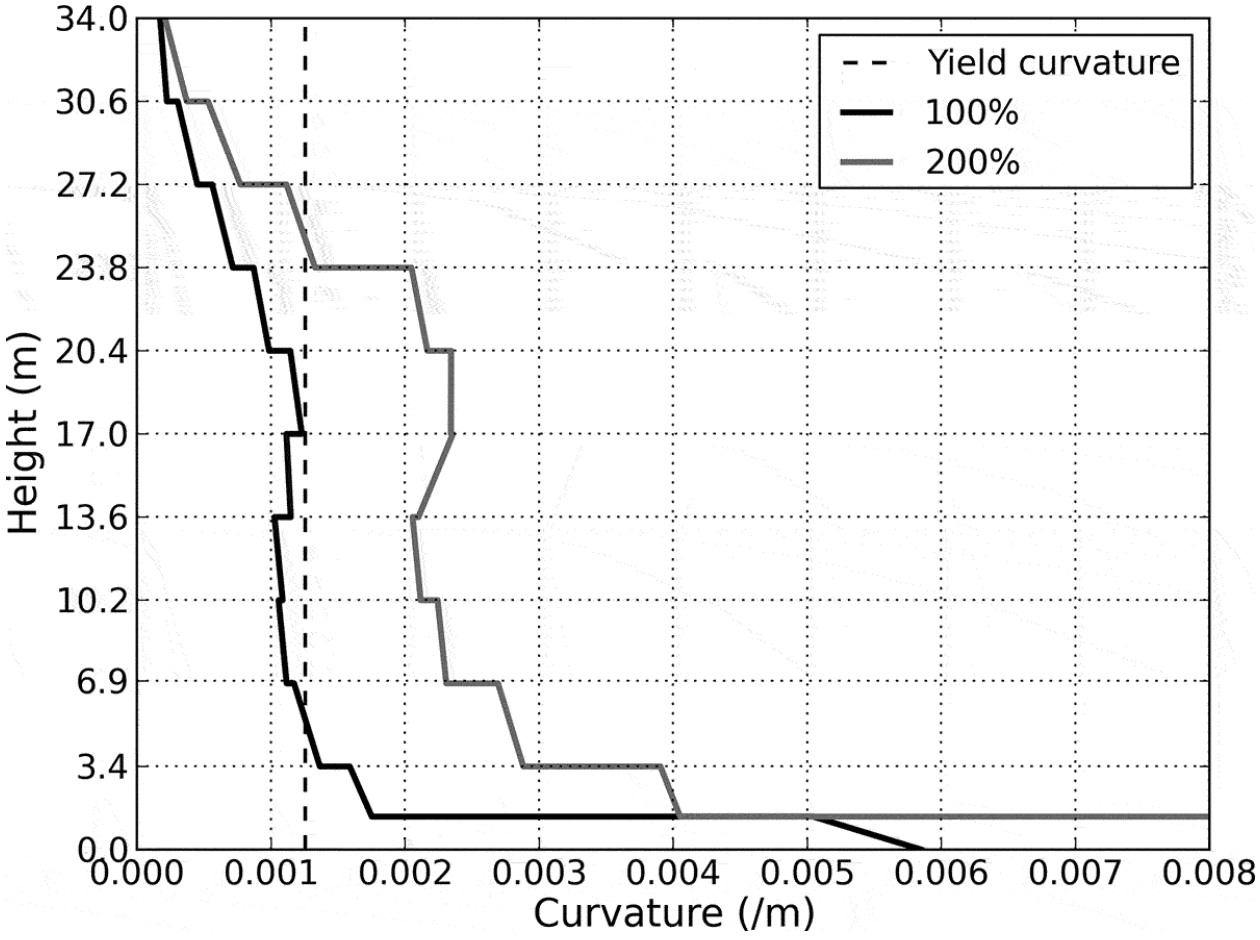

FIGURE 17 Maximum curvature ductility in upper half of walls at (a) 100% intensity and (b) 200% intensity.

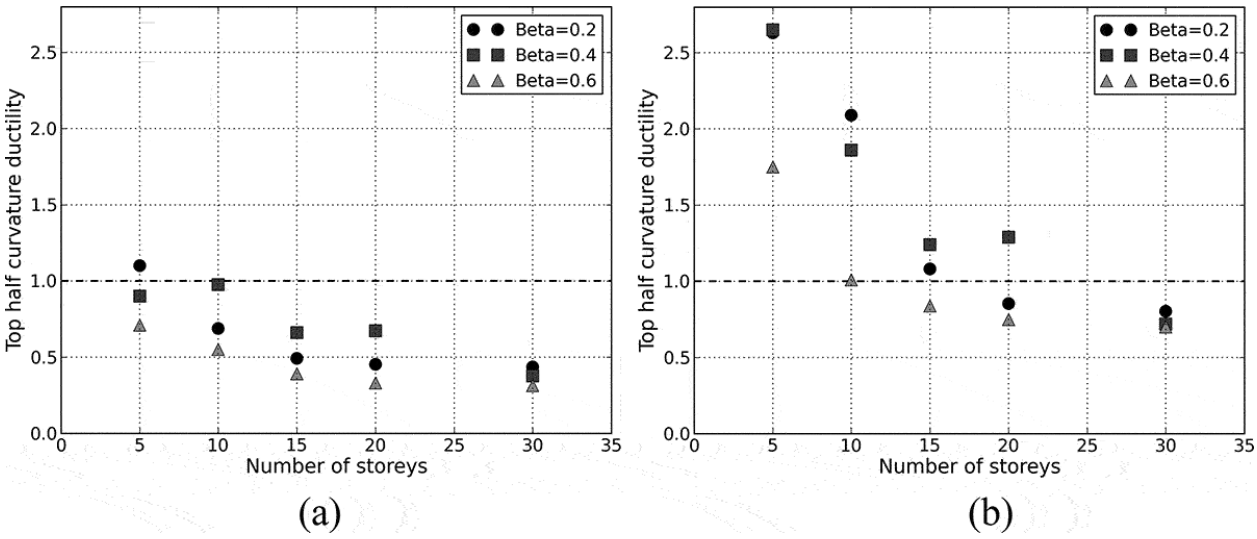

FIGURE 18 Ratio of shear force in individual walls predicted from Equation 29 to the shear force found directly from NTHA for (a) base shear (b) maximum upper half shear.

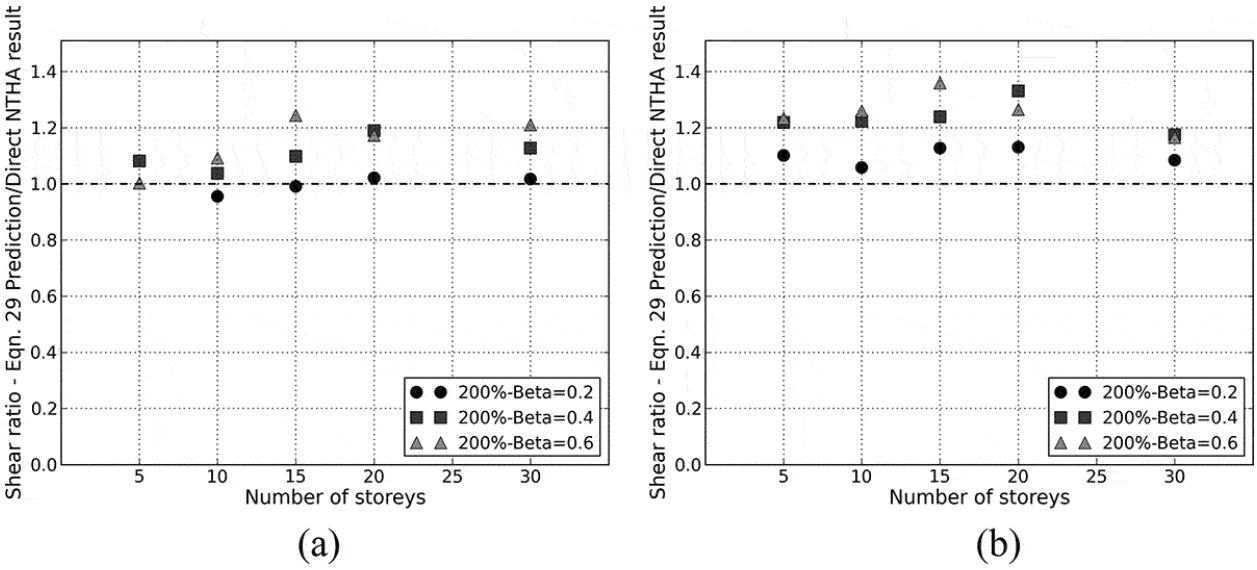

FIGURE 19 Normalised moment demands due to higher modes in cantilever walls for fixed and pinned base components; (a) first higher mode, (b) second higher mode.

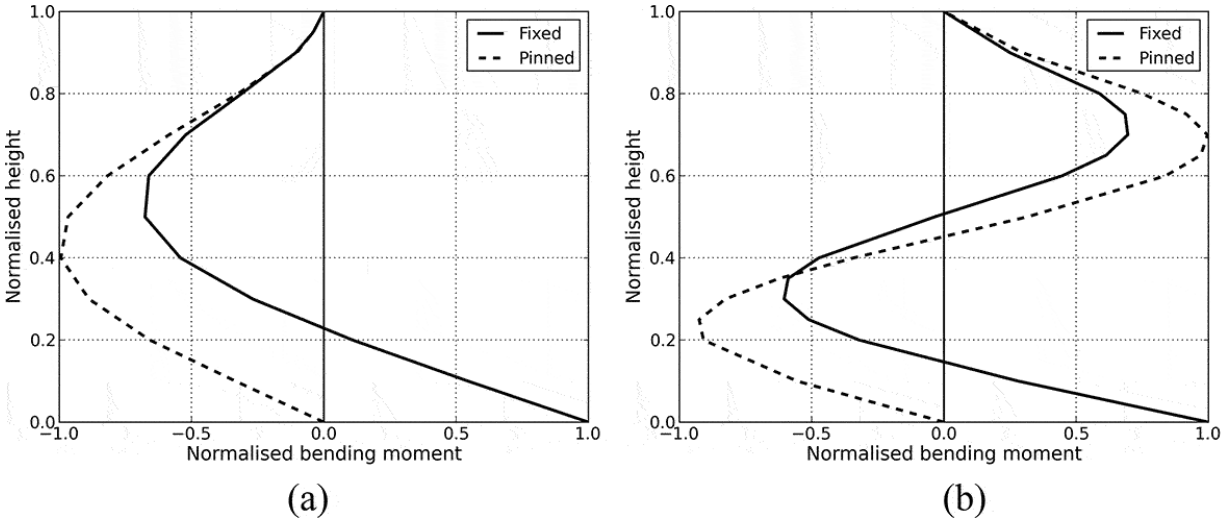

FIGURE 20 Cracked stiffness distribution in coupled walls after coupling beams have yielded (fictitious three storey building).

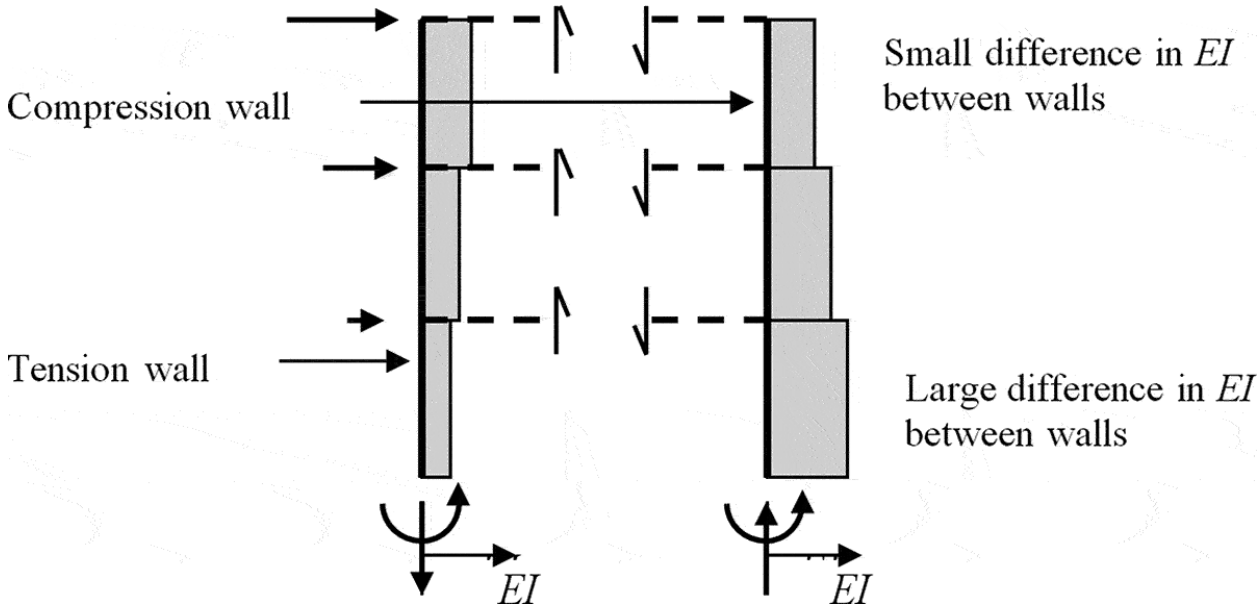

FIGURE 21 Ratio of predicted shear force in individual walls predicted by Equation 31 to the shear force found directly from NTHA for (a) base shear (b) maximum upper half shear.

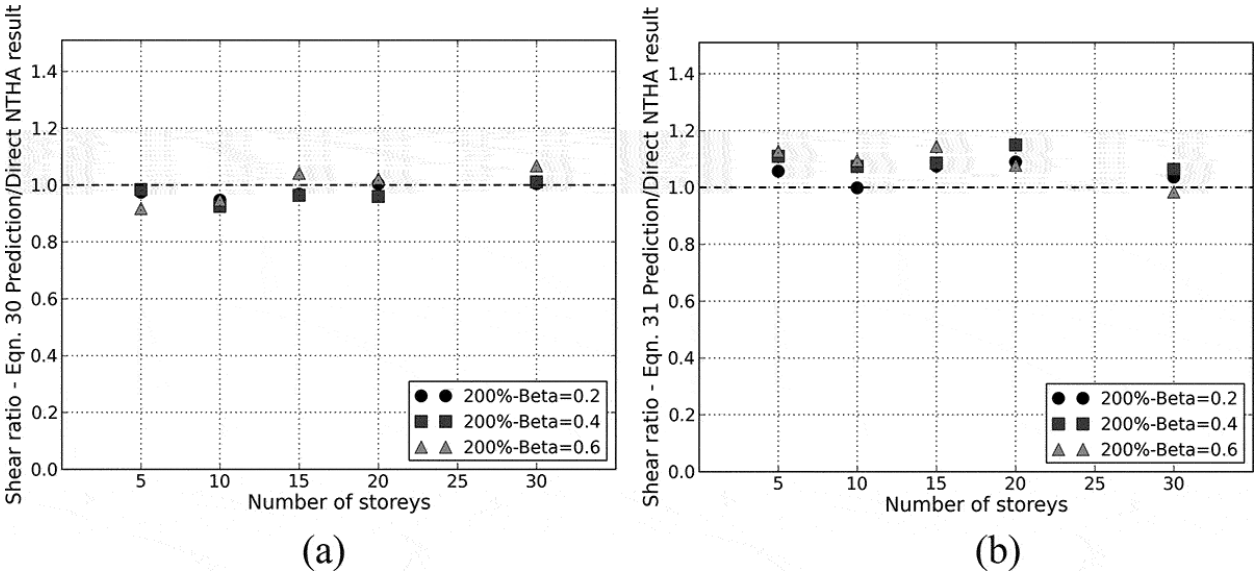

Table 1 Accelerograms used in NTHA.

Earthquake	Station Name	Earthqua	Component	Durati
Chi-Chi, Taiwan	CHY082	7.62	CHICHI/CHY082-	90
Kocaeli	KOERI Botas	7.51	KOCAELI/BTS09	102
Landers	CDMG 14368 Downey - Co	7.28	LANDERS/DWN	70
Hector	Mecca - CVWD Yard	7.13	HECTOR/116250	60
St Elias, Alaska	USGS 2728 Yakutat	7.54	STELIAS/059v22	83.2
Loma Prieta	USGS 1028 Hollister City Hall	6.93	LOMAP/HCH090	39.1
Northridge-01	Neenach - Sacatara Ck	6.69	NORTHR/NEE09	48
Superstition	Westmorland Fire Station	6.54	SUPERST/B-	40
Imperial Valley-	El Centro Array #1	6.53	IMPVALL/H-	39.3
Chi-Chi,	TCU061	6.2	CHICHI03/TCU06	107

Table 2 for use in Appendix A (without header)

	β=0.2					β=0.4					β=0.6				
n	5	10	15	20	30	5	10	15	20	30	5	10	15	20	30
L_w (m)	3	4	6	8	9	2.5	3.5	4.5	8	8.5	1.5	2	2.5	2.8	3.4
t_w (m)	0.25	0.35	0.45	0.65	0.8	0.25	0.3	0.35	0.4	0.7	0.35	0.6	0.8	1	1.6
h_{CB} (m)	0.8	0.8	0.8	0.8	0.8	0.8	0.8	0.8	0.8	0.8	1	1	1	1	1
L_{CB} (m)	2	2	2	2	2.5	2	2	2	2	2	4	4	4	4	4
N_{grav} (kN)	1425	3000	4950	7200	11363	1388	2925	4613	7200	11025	1388	2850	4388	5940	9180
T_1 (s)	1.3	1.8	2.5	3	5.3	1.23	2.2	2.9	3.3	5.9	1.5	2.5	3.9	5.6	9.9
T_e (s)	3.47	5.20	4.21	3.82	7.44	3.71	5.99	6.59	5.07	6.71	3.73	5.98	7.42	9.21	12.98
K_e (kN/m)	5888	4802	10227	15497	6066	5191	3684	4343	9417	7653	5138	3670	3416	2447	1202
V_b (kN)	1749	2544	4839	7047	7038	1609	2202	3206	5244	6525	1629	2228	3000	3243	3847
M_{OTM} (MNm)	22.3	63.1	181.5	357.4	531.6	20.4	54.2	118.4	259.3	488.5	20.7	55.0	111.0	161.4	293.5
M_{wall} (MNm)	8.9	25.3	72.6	143.0	212.7	6.1	16.3	35.5	77.8	146.5	4.1	11.0	22.2	32.3	58.7
V_{CB} (kN)	178	210	303	357	308	363	394	486	519	620	451	550	683	712	793
N_{eq} (kN)	891	2105	4538	7148	9246	1817	3945	7286	10374	18608	2254	5503	10246	14241	23794
$A_{S,CB}$ (mm^2)	649	764	1113	1322	1500	1331	1434	1774	1903	2283	2533	3096	3848	4013	4466
ρ_w	0.0159	0.0185	0.0197	0.0189	0.0208	0.0151	0.0181	0.0214	0.0108	0.0195	0.0235	0.0201	0.0201	0.0264	0.0260